www.lajss.org
Latin American Journal of Solids and Structures 5 (2008) 99–117

Optimization of elastic structures using boundary elements and a topological-shape sensitivity formulation

Rogério José Marczak*

Mechanical Engineering Department, Federal University of Rio Grande do Sul, Porto Alegre - RS, Brazil

Abstract

The objective of this work is to present the implementation of a hard kill material removal algorithm in a standard BEM formulation. A topological-shape sensitivity approach is used to select the points showing the lowest sensitivities, where material is removed by opening a cavity. As the iterative process evolutes, the original domain has holes progressively punched out, until a given stop criteria is achieved. Benchmarks of two-dimensional elasticity are presented and analyzed. Because the BEM does not employ domain meshes in linear cases, the resulting topologies are completely devoid of intermediary material densities. The results obtained showed that the material removal strategy plays a key role in the generation of quality results. Although the drawbacks of hard-kill methods are still present, the present approach opens an interesting field of investigation for integral equation methods, so far accomplished only within the finite element methods context.

1 Introduction

Topology optimization has been a major research subject in many engineering fields during the last decades, and a number of numerical methods has emerged to perform this type of computational design task efficiently. Among these, SIMP (solid isotropic material with penalizaton) methods are possibly the most used approaches for topology optimization of structures. Since the early work of Bendsºe & Kikuchi [3] on homogenization methods, several SIMP techniques and their variants have been developed and successfully used in structural optimization problems [2]. Because SIMP methods deal with variable material densities, the finite element method (FEM) has became the natural choice for the numerical solution of the equations. Additionally, the technique is able to generate globally optimal solutions, i.e. microstrutured designs. Although strictly correct from the mathematical standpoint, this type of solution often fails to generate engineering designs in a straightforward manner. In order to render a 0-1 (void-material) solution, suboptimal microstructures with penalization of the density gradient are used to avoid large areas with intermediate material (fig 1).

Since the material distribution is related to the finite element mesh, results obtained through SIMP methods generally suffer from mesh dependency. Another major drawback of the tech-

*Corresp. author email: rato@mecanica.ufrgs.br Received 8 Jan 2007; In revised form 10 Mar 2008

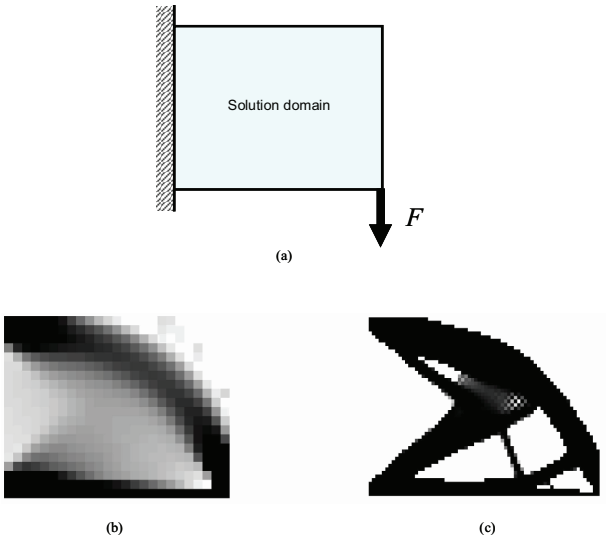

Figure 1: Typical optimization solution obtained with FEM and SIMP methods. (a) Initial problem; (b) Original solution; (c) Penalized solution.

nique arises when some types of density gradient control are applied, possibly generating checkerboard instabilities that must be avoided in order to attain feasible designs (2).

Another alternative method which has also been under development during the last years are the topological derivative (TD) or topological-shape sensitivity methods [6, 15, 16]. This family of methods belongs to the ESO (evolutionary structural optimizaton) type, and aims the elimination of the material density dependency.

Most of the research on topology optimization has been based on FEM methods (see, for instance, [7]). The objective of the present work is to apply a recently developed TD approach with boundary element methods (BEM). A previous BEM methodology developed for heat transfer problems [8] is extended to elasticity problems. Since the BEM does not need domain mesh, its use with TD methods renders a fully 0-1 approach, thus avoiding intermediary material densities and the associated numerical drawbacks. First, a review of the TD formulation adopted herein is addressed, which is particularized for 2D elasticity. Next, a numerical methodology is devised to carry out the computational design by an iterative BEM procedure. A number of examples are solved with the proposed formulation and the results are discussed.

2 A short review of topological-shape sensitivity for 2D elasticity equation

The idea behind topology derivative is the evaluation of a cost function sensitivity to the creation of a new cavity. Wherever this sensibility is low enough the material can be progressively

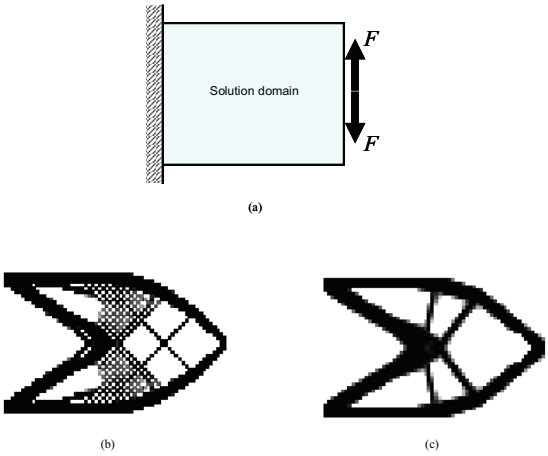

Figure 2: Example of checkerboard instability in optimization solution obtained with FEM and SIMP methods. (a) Initial problem; (b) original (unstable) solution; (c) controlled solution.

eliminated.

The original concept of topological derivative is related to the sensitivity of a given cost function ψ when the topology of the analysis domain Ω is changed by inserting a small hole of radius ε centered on $\hat{\mathbf{x}}$. The local value of the topological derivative at a point $\hat{\mathbf{x}}$ for this case evaluated by:

$$D_T^*(\hat{x}) = \lim_{\varepsilon \to 0} \frac{\psi(\Omega_\varepsilon) - \psi(\Omega)}{f(\varepsilon)} \tag{1}$$

where $\psi(\Omega)$ and $\psi(\Omega_\varepsilon)$ are the cost function evaluated for the original and the changed domain, respectively, and f is a regularizing, problem dependent, function such that $f \to 0$ when $\varepsilon \to 0$. The major drawback of this concept is that it is not possible to establish an isomorphism between domains with different topologies, making the evaluation of Eq.(1) rather difficult or impossible (fig.3).

Feijoo et. al [6] and Novotny et. al [12] circumvented this problem introducing the mathematical idea that the creation of a hole can be accomplished by simply perturbing an existing one, whose radius tends to zero (Fig. 4). Now both domains have the same topology and it is possible to establish a mapping between each other:

$$D_T(\hat{x}) = \lim_{\substack{\varepsilon \to 0 \\ \delta\varepsilon \to 0}} \frac{\psi(\Omega_{\varepsilon+\delta\varepsilon}) - \psi(\Omega)}{f(\varepsilon + \delta\varepsilon) - f(\varepsilon)} \tag{2}$$

where $\delta\varepsilon$ is a small perturbation on the hole's radius. It is important to note that Eq.(2) is formally rendering a shape sensitivity character to the original expression, but it can be proven that the Eqs.(1) and (2) are equivalent. The evaluation of D_T is, however, much easier than its original counterpart D_T^*.

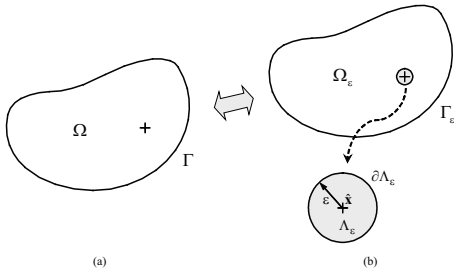

Figure 3: The original concept of topological derivative. (a) Original domain. (b) Perturbed domain.

In the present work, the interest rests on the evaluation of D_T for problems governed by the elasticity operator. Following the work of Novotny et. al [12], the topological derivative equations for linear elasticity will be reviewed. The direct problem is stated as:

$$\text{Find:} \quad \{\mathbf{u}_\varepsilon \,|\text{div}\sigma_\varepsilon = b\} \quad \text{on } \Omega_\varepsilon \tag{3a}$$

$$\text{Subjected to:} \begin{cases} \mathbf{u}_\varepsilon = \bar{\mathbf{u}} & \text{on } \Gamma_u \\ \sigma_\varepsilon \mathbf{n} = \bar{\mathbf{t}} & \text{on } \Gamma_t \\ \sigma_\varepsilon \mathbf{n} = 0 & \text{on } \Gamma_\varepsilon \end{cases} \tag{3b}$$

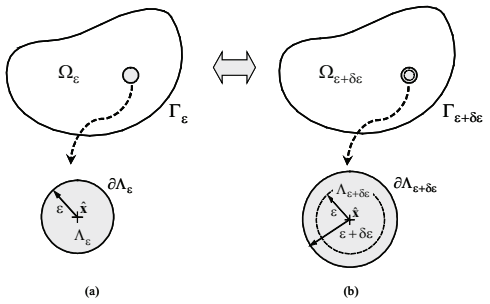

Figure 4: The modified concept of topological derivative. (a) Original domain. (b) Perturbed domain.

Let a general form for cost function be written as total strain energy function:

$$\begin{aligned} \Psi(\mathbf{u}_\tau) =& \frac{1}{2}\int_{\Omega_\tau} \mathbf{C}\nabla_\tau \mathbf{u}_\tau \cdot \nabla_\tau \mathbf{u}_\tau d\Omega_\tau - \int_{\Omega_\tau} \mathbf{b}\cdot\mathbf{u}_\tau d\Omega_\tau - \int_{\Gamma_t} \bar{\mathbf{q}}\cdot\mathbf{u}_\tau d\Gamma_\tau \\ =& \frac{1}{2} a_\tau(\mathbf{u}_\tau, \mathbf{u}_\tau) - l_\tau(\mathbf{u}_\tau) \end{aligned} \tag{4}$$

where τ is the perturbation parameter associated to the shape change velocity (i.e. $\mathbf{x}_\tau(\mathbf{x}) = x + \tau\mathbf{v}(\mathbf{x})$). The sensibility of the cost function with respect to τ can be obtained from the

Gâteaux derivative of the perturbed configuration given by Eq.(4):

$$\frac{d}{d\tau}\Psi\left(\Omega_\tau\right)_{\tau=0} = \lim_{\tau\to 0}\frac{\Psi\left(\Omega_\tau\right) - \Psi\left(\Omega_{\tau|\tau=0}\right)}{\tau} = 0 \text{ on } \partial\Gamma_\varepsilon \tag{5}$$

After an intensive analytical work, the topological derivative results, in absence of body loads:

$$D_T\left(\hat{\mathbf{x}}\right) = -\lim_{\varepsilon\to 0}\frac{1}{f'\left(\varepsilon\right)}\int_{\Gamma_\varepsilon}\frac{1}{2\rho E}\sigma_\varepsilon^{tt}d\Gamma_\varepsilon$$

Using an asymptotic analysis of the solution $\mathbf{u}_\varepsilon$, the following expression is found:

$$D_T\left(\hat{\mathbf{x}}\right) = \frac{2}{1+\nu}\sigma\cdot\varepsilon + \frac{3\nu-1}{2(1-\nu^2)}\mathrm{tr}\sigma\mathrm{tr}\varepsilon \tag{6}$$

which can be particularized for plane strain problems as

$$D_T\left(\hat{\mathbf{x}}\right) = \frac{2}{(1+\nu)(1-2\nu)}\sigma\cdot\varepsilon + \frac{(1-\nu)(4\nu-1)}{2(1-2\nu)}\mathrm{tr}\sigma\mathrm{tr}\varepsilon \tag{7}$$

A similar expression can be derived for the plane stress case. Further details about the derivation of eqs.(6) and (7) can be found in [6].

3 Numerical methodology

In order to evaluate Eq.(7), the BEM was used in its direct version [4, 5]. Since the evaluation of physical variables on internal points with the BEM is a post-processing step, the recovery of local values for D_T can be easily implemented. Furthermore, because the BEM shows better accuracy for the evaluation of boundary variables than other popular methods like the FEM, it is expected a good performance of the approach for boundary points (which is an important issue in shape changes).

1. The optimization process is carried in four basic steps (see Fig. 5):
2. The standard BE problem is solved, and the variables are evaluated on a suitable grid of interior points.
3. The points with the lowest values of D_T are selected.
4. Holes are created by removing material areas centered on the previously selected points.
5. Check stopping criteria, rebuild the mesh, and return to step 1, if necessary.

At this point, the desired topology is expected. It is important to stress that, strictly speaking, the *punching* strategy here adopted is a type of *hard-kill* method for material elimination.

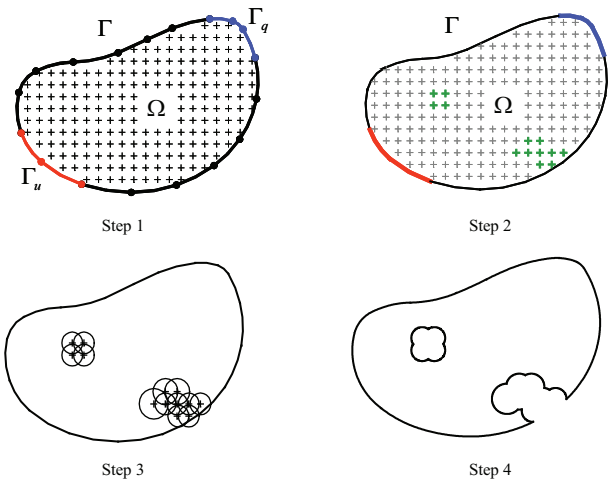

Figure 5: BEM iterative procedure for material removal.

This can be an issue in some non-convex problems, when material creation (filling) may occur simultaneously with material elimination.

It is worth to comment some aspects regarding the step 2. A common drawback in many shape and topology optimization methods is the progressive lost of symmetry in originally symmetric problems. This is related to the numerical evaluation of sensitivities, which are always prone to round-off and truncation errors. The material removal strategy also has influence on the final results, since symmetric topologies demand symmetric elimination of material. The material removal rate has a heavy influence on the computational cost of the analysis. These issues were faced in the early stages of the present work [8], and three strategies were successively devised to overcome it:

- **Method A**: Creation of a single hole per iteration: This is a very crude form of material removal, and computationally very inefficient. The point with the lowest D_T value is used to create the hole. Besides being unable to create more than one hole at each iteration (with obvious lost of symmetry), a large number of iterations is necessary to achieve a given solution.

- **Method B**: Creation of N_h holes per iteration: This is a natural improvement over method A, where a preset number of holes is allowed to be created at each iteration. It is computationally more efficient that its predecessor, but there is no simple way to guarantee symmetric solutions.

- **Method C**: It is a cut-off method: This method was devised to try to remove larger areas of material in each iteration. The ideal solution would be to remove all areas inside the

isolines at a given level of topological derivative, for each iteration. A simpler shortcut is to define a cut-off value:

$$D_{\text{cutoff}} = \min\left(D_T^i\right) + \rho\left[\max\left(D_T^i\right) - \min\left(D_T^i\right)\right] \tag{8}$$

where i =1..number of sampling points (internal and boundary points). Therefore, all points with $D_T \leq D_{\text{cutoff}}$ are used to remove material.

After a number of preliminary tests, the methods B and C were found to be the best ones, and it was used throughout this work. By selecting suitable values of ρ, the rate of material removal can be controlled, provided it is not very large. Values in range $0.2\% \leq \rho \leq 5\%$ proved to be sufficient for most applications.

4 Numerical results

This section presents a number of cases analyzed using the proposed formulation. These are initial results, used to test the formulation. Traction free boundary conditions were employed on the holes. In all cases, the total potential energy was used as the cost function. The total amount of material removed was checked at the end of each iteration and compared to a reference value until the desired volume is achieved. All cases used linear discontinuous boundary elements integrated with 8 Gauss points. The regularly spaced grid of internal points was generated automatically, taking into account the radius of the holes to be created during each iteration. The radius was taken as a fraction of a reference dimension of the domain ($r = \alpha l_{\text{ref}}$). They may vary in order to accelerate or decelerate the material removal rate, but usually $l_{\text{ref}} = \min(H, L)$ was adopted, where H and L are the height and length of the domain. The material volume is to be minimized in all cases. The current area of the domain (A_f) was checked at the end of each iteration until a reference value is achieved ($A_f = \beta A_0$, where A_0 is the initial value). The examples shown in this section employed circular holes discretized with six boundary elements.

4.1 Benchmark 1 - Fixed support

In this case a square domain has its left edge clamped and is subjected to a load on its upper right corner (Fig.6). Holes with fixed radius were used throughout the process ($r = 0.025a$).

The evolution history is shown in Fig.7, for $N_h = 4$. The process was halted when $A_f = 0.4A_0$ was reached. Figure 8 shows the results obtained for this case when $N_h = 8$. Both cases delivered the same topologies, but evidently the solution was much faster in the latter one.

The results of Figures 7 and 8 show clearly that the use of hexagon-shaped holes, along with internal points meshes not sufficiently refined deliver very irregular boundaries. although not the main focus of the present work, it is important to note that better results can be obtained with different *punching* procedures. This benchmark was re-analyzed using a regularly spaced internal points mesh and quadrilateral holes. The spacing between the internal points was specified in

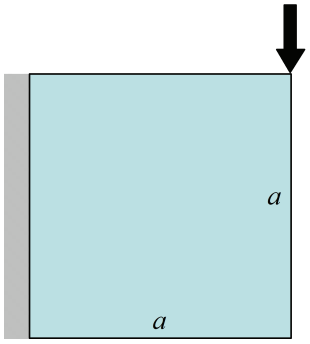

Figure 6: Illustration of benchmark 1.

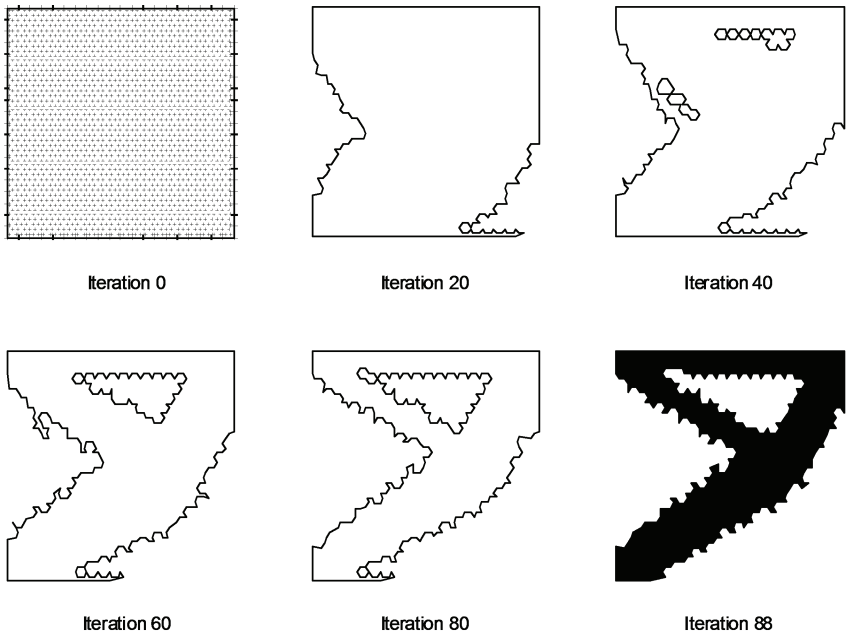

Figure 7: Optimization history of benchmark 1 – Method B with $N_h = 4$.

such a way that there is no overlap between two holes. This type of material removal procedure was tested in heat transfer problems before [8], and results in a tiled pattern for the holes, similar to FEM designs in SIMP methods. This procedure was developed to remove the jagged edges of the boundary. Results for $r = 0.035a$ are shown in Fig.9.

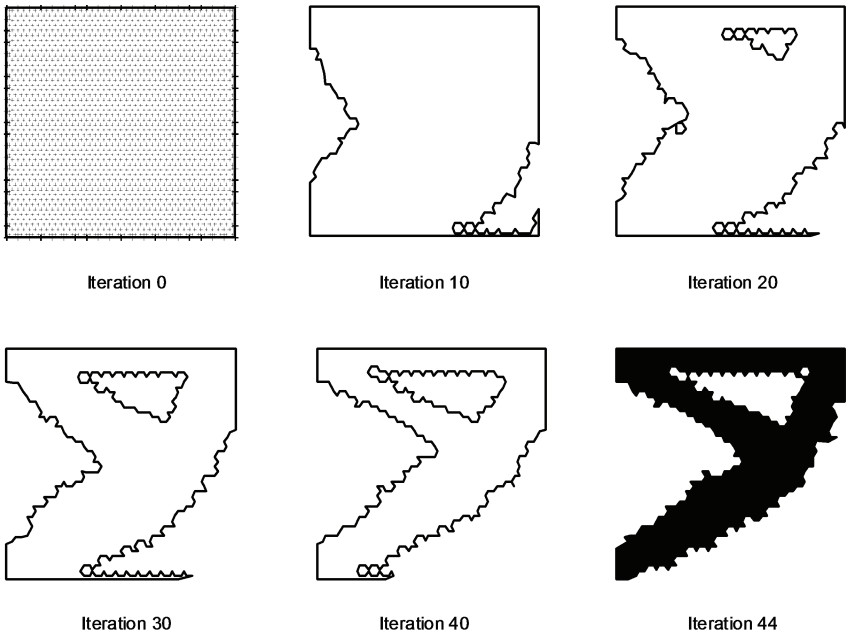

Figure 8: Optimization history of benchmark 1 – Method B with $N_h = 8$.

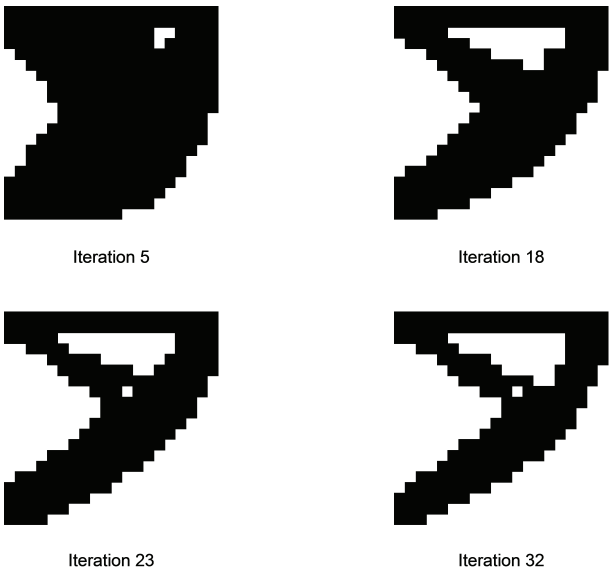

Figure 9: Optimization history of benchmark 1 – Method B with $N_h = 8$ using tile pattern and rectangular holes.

4.2 Benchmark 2 - Cantilever beam

In this case rectangular cantilever structure has its left edge clamped and is subjected to a load on its upper right corner (Fig. 10). Three different solution strategies were used to solve this problem.

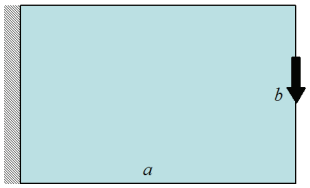

Figure 10: Illustration of benchmark 2.

The first solution used $r = 0.04a$ and method C with a fixed value of ρ in Eq.(8). The evolution history is shown in Fig. 11. Because a larger hole was used, the algorithm eliminated material very fastly, resulting a slender design with $A_f = 0.15A_0$ after 57 iterations.

The second solution used $r = 0.03a$ and method B with $N_h = 12$. As shown by the evolution history in Fig. 12, in this case the smaller radius of the holes and the more controlled material removal provided by method B allowed the formation of internal reinforcement bars, similar to those also found in FEM solutions [1, 2]. The process was halted in the 40^{th} iteration, when $A_f = 0.35A_0$.

The third solution repeated the last one, but using a slightly more dense internal points grid. As a consequence, the D_T sampling space was enriched and a more refined reinforcement pattern was found (Fig. 13).

The final design took 32 iterations to reach $A_f = 0.45A_0$. This dependence is deeply rooted in the existence of a global optimum, which is microstructured. As the internal mesh is refined (and the holes radius decreased) the likelihood of finding a microstructured solution also increases.

This is in good agreement with similar results obtained with the FEM [14], but still suffers from jagged edges and non-physical appendices. Again, this can be solved by using tiled holes. Figure 14 exemplifies the results obtained with the tiling procedure which, again, resamble SIMP-like results.

4.3 Benchmark 3 - Michell truss

In this case refers to the popular Michell truss [11, 13]. The geometry, boundary conditions and loading for this benchmark are depicted in Fig. 15*a*. Two possible optimal solutions are shown in Fig. 15*b*. The theoretical solutions of Fig. 15*b* have their configurations dependent on the number of bars used.

This case was initially analyzed with the proposed formulation using method B with $r = 0.02a$ and $N_h = 8$. The corresponding optimization history is depicted in Fig. 16. This case

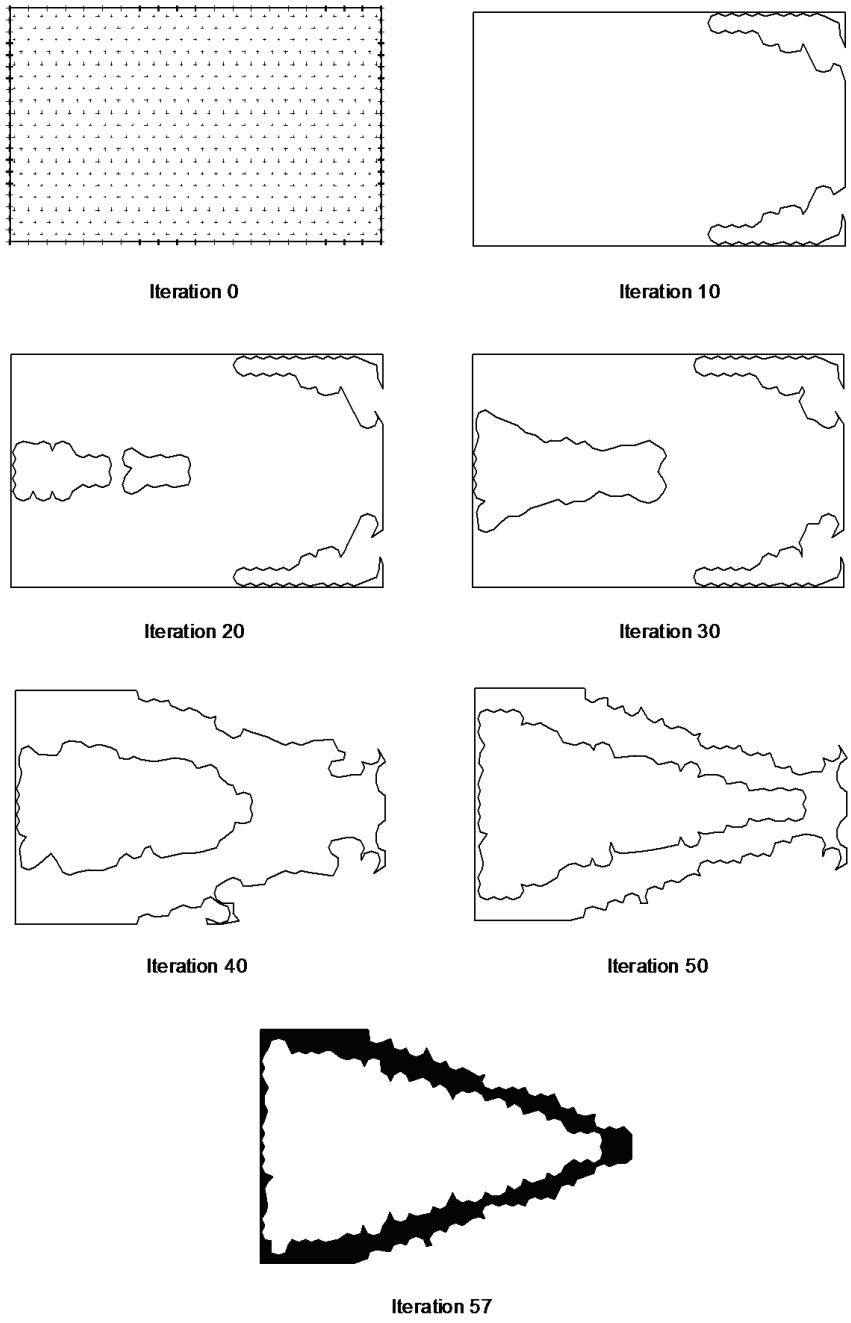

Figure 11: Optimization history of benchmark 2 - Method C with $r = 0.04a$.

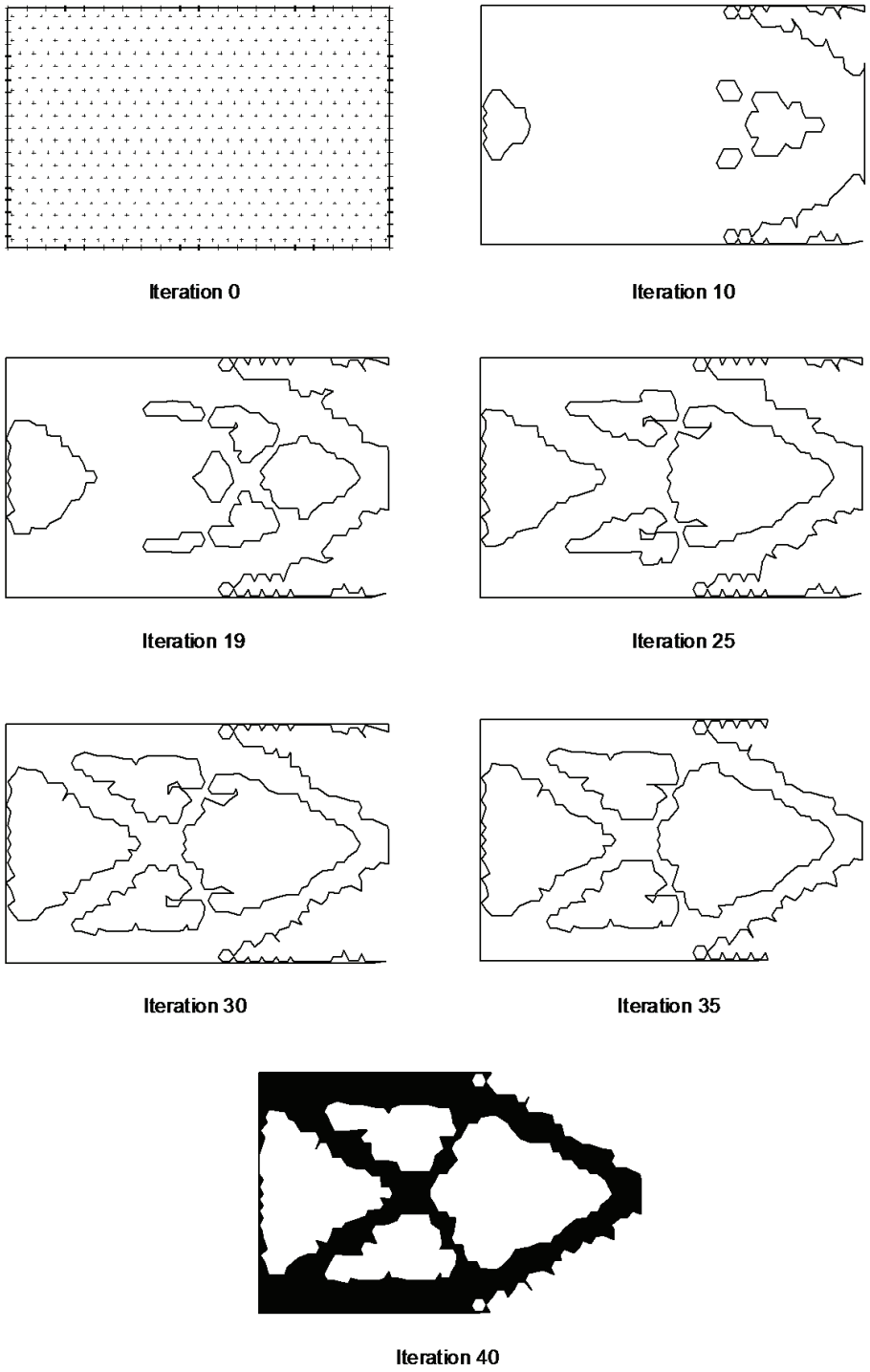

Figure 12: Optimization history of benchmark 2 - Method B with $r = 0.04a$ and $N_h = 12$.

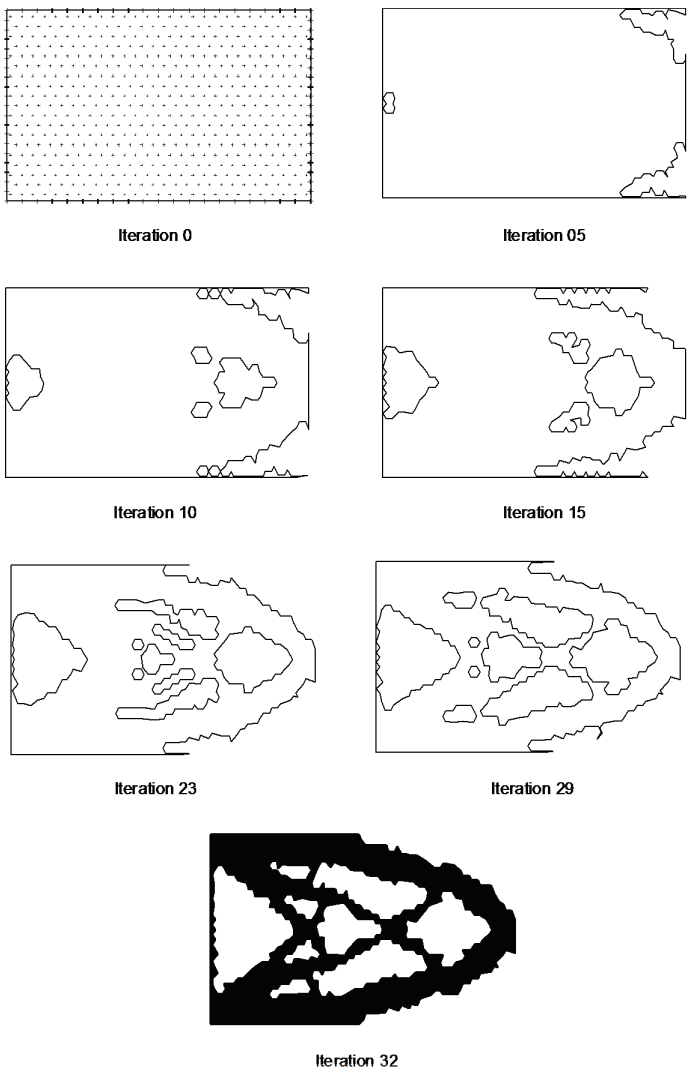

Figure 13: Optimization history of benchmark 2 - Method B with $r = 0.03a$ and $N_h = 12$.

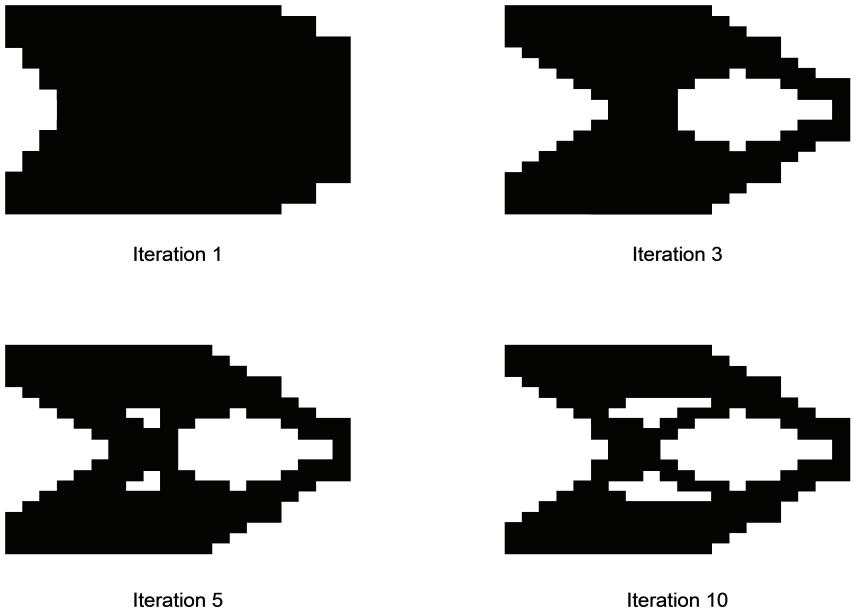

Figure 14: Optimization history of benchmark 2 - Method B with $r = 0.05a$ and $N_h = 24$ using tile pattern and rectangular holes.

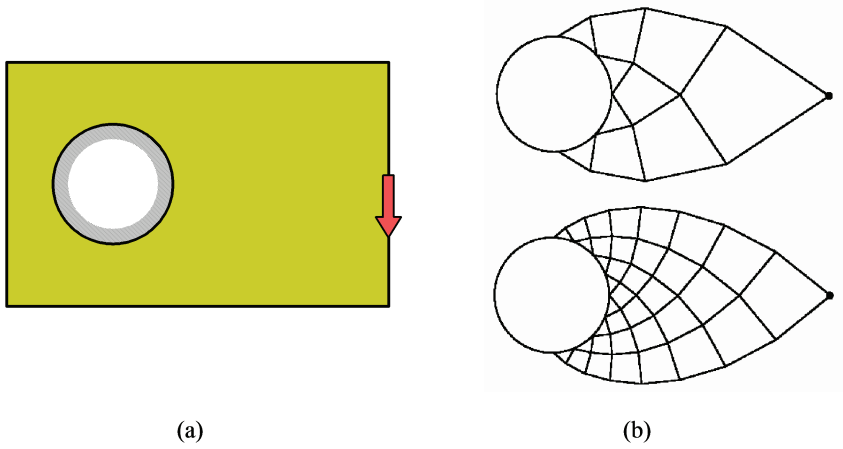

Figure 15: (a) Illustration of benchmark 3. (b) Theoretical optimal solution (Michell truss).

shows clearly that reinforcement bars result more heavily affected by thin appendices, although rougly resembling the structure of Fig. 15*b*. Evidently, the use of the tiling procedure reduces the effect, as shown in Fig.17.

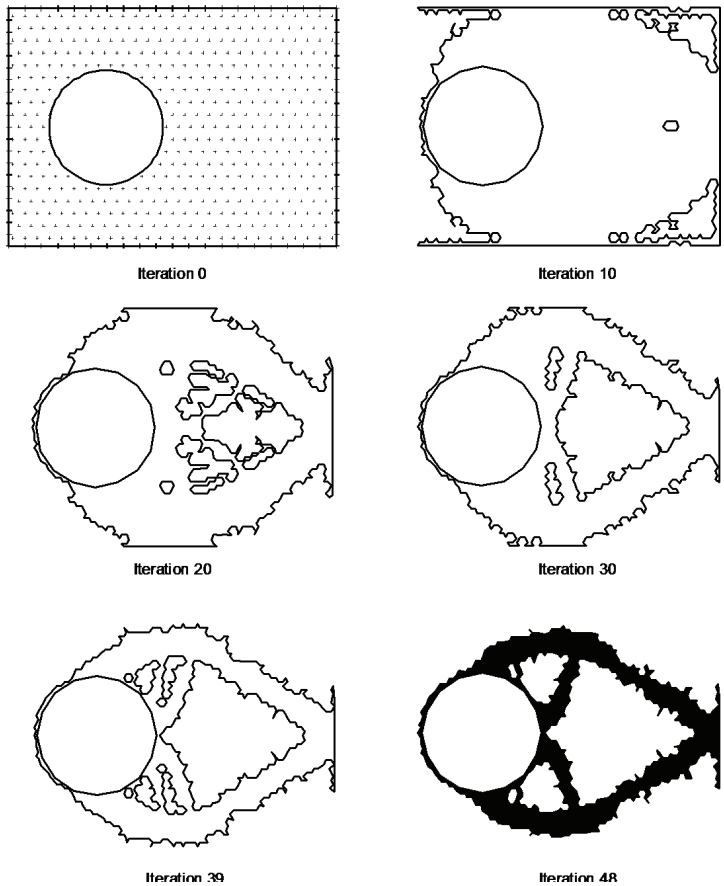

Figure 16: Optimization history of benchmark 3 - Method B with $r = 0.02a$ and $N_h = 8$.

5 Additional comments

The results presented in the previous section show clearly that, although useful results can be obtained with the proposed methodology, it shares the very same problems of most hard kill methods. If conveniently controled, the designs thus obtained are acceptable, but it may be virtually impossible to specify a sufficiently general material removal rule regardless the

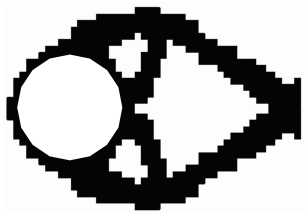

Figure 17: Final design of benchmark 3 (iteration 42) - Method B with $r = 0.04a$ and $N_h = 8$.using tile pattern and rectangular holes.

application. Furthermore, the imposition of restrictions to the problem is rather complex, since the analytical expressions for D_T have been derived without considering them.

A major issue in the present formulation is related to the relative magnitude of the D_T values as the iterative process evolves. After the first few iterations, the gradient of D_T along the domain becomes very low, since the optimal solution has constant D_T. Considering that some areas of the domain may be more affected by modeling and discretization errors than others, a fine tuning becomes mandatory to avoid material rejection at non-optimal locations. The other issue is related to the (non-mathematical) stopping criteria used. Specified volume fractions are relatively easy to implement. In the present approach, the current volume is compared with the target volume at the end of each iteration, and the process is halted if necessary (this is possible because the number of holes and the diameters are known during run time). Although useful for material saving, this criteria is devoid of further information like energy content or compliance values.

If, by one side, ESO methods like the one presented here show serious limitations, on the other side one can make interesting usages of D_T, particularly in conjunction with other optimization methods. For instance, if a surface of D_T values is contructed, its isolines could be used to specify a material rejection criteria. Figure 18 shows the case of benchmark 1, where a map of normalized D_T values was plotted for the original domain. All material inside isolines with a specified treshold value (12%, in the example) was removed by intersecting the D_T map with the original domain. In the first iteration, the areas with the lowest sensitivities are still very clear. However, since the normalization is kept constant, these areas become less evident in the next iteration, and the intersection of the isolines (keeping the same treshold value) with the previous domain results in less material removal. This is expected, as discussed above, and depending on the treshold value the intersection may not happen at all. However, the domain obtained after the first iteration can be a good starting point for SIMP methods or a shape optmization analysis. Figure 19 presents similar results obtained for benchmark 2, and exemplifies the fast decay in the gradients of D_T after the first pass. Although these results present smoother boundaries than the ones presented in the previous section, finding a general rejection criteria based solely on treshold values seems an impossible task.

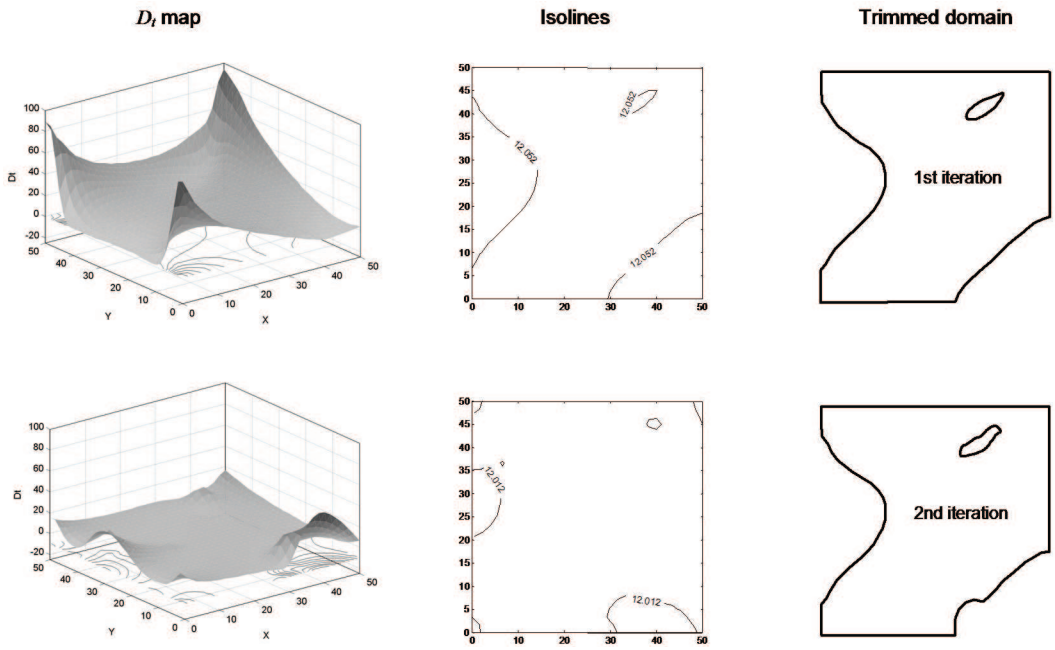

Figure 18: Designs obtained using D_T isolines as a rejection criteria for benchmark 1.

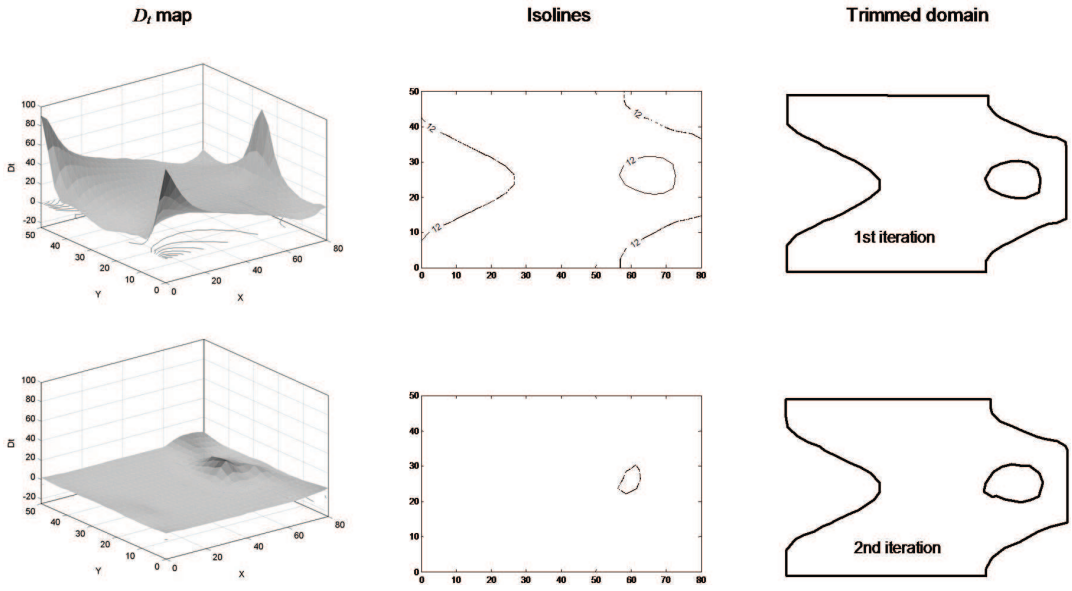

Figure 19: Designs obtained using D_T isolines as a rejection criteria for benchmark 2.

Another point to be highlighted here is possibility of using of post-processing algorithms to smooth the boundaries obtained not only with the BEM methodology shown here, but also to eliminate the see-saw aspect of most SIMP approaches reported. Line simplification or line generalization algorithms encompass a family of tools largely used in cartographic and geographic applications, and can be used to render topology optimization solutions more close to the actual manufacturing designs [9, 10].

Finally, it is worth to point out that the tiling scheme generates solutions very similar to the ones obtained with SIMP methods. Obviously the size of the tiles must be reduced in order to increase the resolution of the boundaries. This will reflect heavily on the number of internal points used to evaluate the sensitivities, and consequently will increase the computational cost of the BEM analysis.

6 Conclusions

The present approach has presented essentially the application of a hard kill strategy for topology optimization of 2D elasticity problems using the boundary element method. The relevant expressions for topological derivative evaluations are reviewed, aiming their implementation for problems governed by plane stress or plane strain equations. The formulation is derived by introducing a specially devised iterative material removal procedure in a BEM framework. Some classical benchmark cases are solved in order to verify the feasibility of the proposed procedure. Because the BEM does not employ domain meshes in linear cases, the resulting topologies are completely devoid of intermediary material densities. Two schemes for material removal are tested, one based on puching out discs of material, and other based on the removal of non-intersecting tiles of material. While the first generated designs containing very jagged boundaries, the later produced results very similar to those obtained with SIMP methods. Both, however, show the well known problems associated with hard-kill methods.

It is important to mention that the topological derivate approach presented herein is not a well posed problem from the optimization point of view. The cost function (potential energy density) is not explicitly given, and extensions of the formulation to other types cost function will demand elaborate analytical derivations. The imposition of constraints also deserves further investigation.

The presented results proved that the formulation has potential to be used in conjunction with other optimization methods, but its general application as a standalone method must be based on a more mathematically established stopping criteria and material rejection rules. Maybe more important, it opens an interesting field of investigation for integral equation methods, so far accomplished only within the finite element methods context.

References

[1] M. Bends∅e. *Methods for Optimization of Structural Topology, Shape and Material*. Springer-Verlag, New York, 1995.

[2] M. Bends∅e and O. Sigmund. *Topology Optimization. Theory, Methods, and Applications*. Springer-Verlag, New York, 2003.

[3] M.P. Bends∅e and N. Kikuchi. Generating optimal topologies in structural design using a homogenization method. *Comput. Methods Appl. Mech. Engrg.*, 71:197–224, 1988.

[4] C.A. Brebbia and J. Dominguez. *Boundary Elements - An Introductory Course*. Computational Mechanics Publications, Southampton, 1989.

[5] C.A. Brebbia, J.C.F. Telles, and L.C. Wrobel. *Boundary Element Techniques – Theory and Applications in Engineering*. Springer-Verlag, Heildelgerg, 1984.

[6] R. Feijoo, A. Novotny, C. Padra, and E. Taroco. The topological-shape sensitivity analysis and its applications in optimal design. In S. Idelsohn, V. Sonzogni, and A. Cardona, editors, *Mecanica Computacional, volume XXI*, pages 2687–2711, Santa Fe-Parana, Argentina, 2002.

[7] J. Mackerle. Topology and shape optimization of structures using FEM and BEM – a bibliography (1999–2001). *Finite Elements in Analysis and Design*, 39:243–253, 2003.

[8] R. Marczak. Topology optimization and boundary elements – a preliminary implementation for linear heat transfer. *Eng Anal Bound Elem*, 31:793–802, 2007.

[9] R. Marczak and E.L. Cardoso. Application of Line Generalization Algorithms for Boundary Smoothing in FEM and BEM Optimization Solutions. In Brazilian Assoc. for Comp. Mechanics & Latin American Assoc. of Comp. Methods in Engineering, editor, *Proc. XXVI Iberian Latin-American Congress on Computational Methods in Engineering*, Guarapari, Brazil, 2005.

[10] R. Marczak and E.L. Cardoso. Application of genetic algorithms for boundary description in topology optimization solutions. In Brazilian Assoc. for Comp. Mechanics, editor, *Proc. XXVII Iberian Latin-American Congress on Computational Methods in Engineering*, Belém, Brazil, 2006.

[11] A.G.M. Michell. The limits of economy in frame structures. *Phil. Mag.*, 8:589–597, 1904.

[12] A. Novotny, R. Feijoo, E. Taroco, and C. Padra. Topological-shape sensitivity analysis. *Comput. Methods Appl. Mech. Engrg.*, 192:803–829, 2003.

[13] M. Ostoja-Starzewskiy. Michell trusses in the presence of microscale material randomness: limitation of optimality. *Proc. R. Soc. Lond.*, A 457:1787–1797, 2001.

[14] O. Sigmund and J. Petersson. Numerical instabilities in topology optimization: A survey on procedures dealing with checkerboards, mesh dependencies and local minima. *Structural Optimization*, 16:68–75, 1998.

[15] J. Sokoℓowski and A. Żochowski. On topological derivative in shape optimization. research report, 3170. Technical report, INRIA-Lorraine, France, 1997.

[16] J. Sokoℓowski and A. Żochowski. Topological derivatives of shape functionals for elasticity systems. *Mech. Struct. Mach.*, 29:331–349, 2001.